JOURNAL OF COMPUTATIONAL PHYSICS **123,** 74–83 (1996)
ARTICLE NO. 0006

Multidimensional Flux-Limited Advection Schemes

JOHN THUBURN

Centre for Global Atmospheric Modelling, Department of Meteorology, University of Reading, Reading RG6 6AU, United Kingdom

Received December 22, 1994; revised April 18, 1995

A general method for building multidimensional shape preserving advection schemes using flux limiters is presented. The method works for advected passive scalars in either compressible or incompressible flow and on arbitrary grids. With a minor modification it can be applied to the equation for fluid density. Schemes using the simplest form of the flux limiter can cause distortion of the advected profile, particularly sideways spreading, depending on the orientation of the flow relative to the grid. This is partly because the simple limiter is too restrictive. However, some straightforward refinements lead to a shape-preserving scheme that gives satisfactory results, with negligible grid-flow angle-dependent distortion. © 1996 Academic Press, Inc.

1. INTRODUCTION

The advection of a substance with mass mixing ratio q by a fluid of density ρ and velocity $\mathbf{v}$ can be represented either by the flux form of the advection equation,

$$\frac{\partial}{\partial t}(\rho q) + \nabla \cdot (\rho \mathbf{v} q) = 0, \tag{1}$$

or by the advective form,

$$\frac{Dq}{Dt} = 0, \tag{2}$$

where D/Dt means the material derivative;

$$\frac{D}{Dt} \equiv \frac{\partial}{\partial t} + \mathbf{v} \cdot \nabla. \tag{3}$$

The two forms are equivalent when the mass of the fluid is conserved; (1) can be obtained from (2) and vice versa using

$$\frac{\partial \rho}{\partial t} + \nabla \cdot (\rho \mathbf{v}) = 0. \tag{4}$$

But the two forms highlight different properties of the physical process of advection.

The flux form implies that the advected substance can be neither created nor destroyed by the advection; it can only be transported from one place to another through a continuous part of the intervening space. The flux form is a conservation law in the sense of theoretical physics. One corollary is that the total amount of the advected substance, $\int \rho q dV$, is not changed by the advection (given suitable boundary conditions).

The advective form states that the mixing ratio does not change following a fluid parcel. This implies that extrema in the mixing ratio distribution are not amplified. For brevity, this will be referred to as the shape preservation property. Two corollaries of this are (i) that a spatially homogeneous mixing ratio remains spatially homogeneous and (ii) that if the mixing ratio is initially positive everywhere then no negative mixing ratios are produced.

For many applications both the conservation property and the shape preservation property are highly desirable in a numerical advection scheme. In particular, the shape preservation property goes a long way towards ensuring that the numerical method does not generate any spurious oscillations or unphysical negative mixing ratios in the advected field. (However, it does not preclude the generation of spurious changes of gradient, which is sometimes described as ''staircasing.'')

Conservative, shape preserving schemes for one-dimensional problems have been known for some time. One approach for constructing such schemes, called ''flux-corrected transport'' (FCT), e.g., [2–4], involves two stages. A first-order upwind scheme, which is shape preserving but diffusive, is used to advect the field. Then an antidiffusive correction is applied. By carefully constraining, or ''limiting,'' the antidiffusive fluxes the scheme as a whole can be made to retain the shape preservation property. A second, conceptually similar, approach is to use a single stage in which the full fluxes are carefully constrained using a ''flux limiter,'' e.g., [8, 13, 15]. (In the literature there is some interchanging of the terminology, but in this paper ''FCT'' will refer only to the two-stage approach and a ''flux-limited scheme'' will refer only to the single-stage approach.)

Multidimensional advection problems can be solved by time splitting, using a one-dimensional scheme in each coordinate direction. However, this may give unsatisfactory results, particularly for flows with strong deformation [5, 6, 10, 11]. So for many applications genuinely multidimensional shape preserving schemes are preferable. Moreover, many grids, including

0021-9991/96 $12.00

unstructured grids, do not lend themselves to time splitting, so for these grids genuinely multidimensional schemes must be used.

The two-stage FCT approach has been extended to more than one dimension [16] and has been applied successfully to some problems in geophysical fluid dynamics, e.g., [1, 11, 12]. Some progress has been made in extending the single-stage flux-limiter approach to more than one dimension [9]. However, the simplest multidimensional flux-limited schemes, although shape-preserving in the sense defined above, can distort the advected field in a way that depends on the orientation of the flow relative to the grid. Adding certain transverse gradient terms after applying the flux limiter reduces this problem, although the method becomes complicated for a spatially varying flow field.

In this paper a general prescription is given for building shape-preserving schemes using flux limiters in several dimensions and on arbitrary grids (Section 4). The method applies equally well for an advected scalar in either compressible or incompressible flow. Furthermore, with a minor modification it can be applied to the fluid density itself (Section 6). When used on a regular square grid, one of the simplest possible limiters turns out to be too restrictive and leads to a flow-grid angle-dependent distortion similar to that described in [9]. However, the limiter can be refined by taking into account information from upstream diagonal neighbours and by using the available information to relax the limiter at the outflow faces (Section 4.2). The resulting scheme performs well for a range of grid–flow angles, giving minimal distortion of the advected profile. The results are summarized in Section 7.

2. THE BASIC ADVECTION SCHEME

A flux-limited advection scheme consists of a basic advection scheme plus the flux limiter. Usually, a more accurate basic scheme leads to a more accurate flux-limited scheme. This section describes the discrete update equations for density and mass mixing ratio and the basic two-dimensional advection scheme used throughout this paper.

The discrete version of the mass continuity equation, (4), is

$$\rho_k^{m+1} = \rho_k^m + \sum_{\text{in}} c_i \hat{\rho}_i - \sum_{\text{out}} c_j \hat{\rho}_j, \tag{5}$$

where $\sum_{\text{in}}$ means a sum over the inflow faces of the kth grid box and $\sum_{\text{out}}$ means a sum over the outflow faces, ρ_k^m is the average density in the kth grid box at time step m, and a circumflex indicates a value at the face of a grid box. c_i is a Courant number for the flow normal to the ith face of the box:

$$c_i = \frac{|v_i^{(n)}|\gamma_i \,\Delta t}{A_k}. \tag{6}$$

Here, $v_i^{(n)}$ is the normal component of the velocity at the ith face, γ_i is the length of the ith face, A_k is the area of the kth grid box, and Δt is the time step. (In three dimensions γ_i and A_k are the face area and box volume, respectively. In one dimension γ_i is set to 1 and A_k is the length of the grid box.) Note that each face has two Courant numbers, one with respect to the box on each side, and, in general, these may be different if the box areas are different. In fact, for the regular grid used in this paper, γ_i and A_k are constants. However, each face has only one value of $\hat{\rho}$. The method for choosing the values of $\hat{\rho}$ has not yet been specified. Clearly, (5) conserves the total mass of the fluid, $\sum_k \rho_k A_k$, irrespective of how the values of $\hat{\rho}$ are chosen. (To see this, multiply (5) by A_k and sum over k, and use the fact that each face is counted once as an inflow face and once as an outflow face so that the two contributions cancel.)

Similarly, (1) can be discretized to give

$$s_k^{m+1} = s_k^m + \sum_{\text{in}} c_i \hat{s}_i - \sum_{\text{out}} c_j \hat{s}_j, \tag{7}$$

where $s = \rho q$. Each face has only one value of $\hat{s}$, and therefore (7) conserves the total mass of tracer, $\sum_k s_k A_k$, irrespective of how the values of $\hat{s}$ are chosen.

If q_k is defined to be the mass-weighted box average tracer mixing ratio then $s_k = \rho_k q_k$. Also, $\hat{s}$ can be related to a box face mixing ratio by defining $\hat{s}_i = \hat{\rho}_i \hat{q}_i$. Then (7) becomes

$$\rho_k^{m+1} q_k^{m+1} = \rho_k^m q_k^m + \sum_{\text{in}} c_i \hat{\rho}_i \hat{q}_i - \sum_{\text{out}} c_j \hat{\rho}_j \hat{q}_j. \tag{8}$$

Dividing through by (5) gives

$$q_k^{m+1} = \frac{q_k^m + \sum_{\text{in}} \tilde{c}_i \hat{q}_i - \sum_{\text{out}} \tilde{c}_j \hat{q}_j}{1 + \sum_{\text{in}} \tilde{c}_i - \sum_{\text{out}} \hat{c}_j}, \tag{9}$$

where

$$\tilde{c}_i = c_i \hat{\rho}/\rho_k^m \tag{10}$$

is a modified Courant number. Again, each face has two Courant numbers, one with respect to the box on each side, and in general these may be different, even on a uniform grid. A special case is that of a fluid of constant density for which $\tilde{c}_i = c_i$. For such a fluid $\nabla \cdot \mathbf{v}$ must vanish; the discrete analogue of this condition is that the denominator in (9) should be identically equal to 1. Equation (9) is used to update the mixing ratio.

For most of this paper it is assumed that the mass fluxes $\hat{\rho} v^{(n)}$ are known and the task is to choose the values of $\hat{q}$ that give an accurate shape-preserving scheme. In Section 6 we return to the problem of choosing $\hat{\rho}$ given the fluid velocity. In a more general problem the fluid velocity is given and the task is first to choose values of $\hat{\rho}$, allowing mass fluxes to be calculated, and then to choose $\hat{q}$.

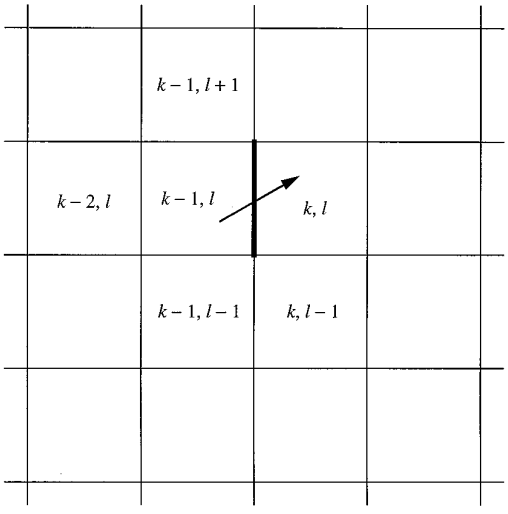

FIG. 1. Schematic showing the stencil of grid boxes used by the basic UTOPIA scheme to calculate the interfacial mixing ratio at the face indicated by the heavy line when the flow at that face is in the direction shown by the arrow.

The basic advection scheme used throughout this paper is the UTOPIA scheme [9], (see also [11]), for a square grid, $\Delta x = \Delta y$. It is based on the idea of two-dimensional cubic upwind interpolation to a parcel's departure point. Reexpressed in terms of the flux form of the advection equation, an interfacial value, $\hat{q}$, for the vertical face between box $(k-1, l)$ and box (k, l), for $c_x > 0$ and $c_y > 0$, as shown in Fig. 1 is given by

$$\hat{q} = \mathrm{LIN} - \frac{|c_x|}{2}\mathrm{GRADN} - \frac{(1-c_x^2)}{6}\mathrm{CURVN} - \frac{|c_y|}{2}\mathrm{GRADT} - \frac{|c_y|}{4}((1-|c_y|)\,\mathrm{CURVT} + (1-|c_x|)\,\mathrm{TWIST}) \tag{11}$$

where

$$\mathrm{LIN} = (q_{k-1,l} + q_{k,l})/2, \tag{12}$$

$$\mathrm{GRADN} = q_{k,l} - q_{k-1,l}, \tag{13}$$

$$\mathrm{CURVN} = q_{k,l} - 2q_{k-1,l} + q_{k-2,l}, \tag{14}$$

$$\mathrm{GRADT} = q_{k-1,l} - q_{k-1,l-1}, \tag{15}$$

$$\mathrm{CURVT} = q_{k-1,l+1} - 2q_{k-1,l} + q_{k-1,l-1}, \tag{16}$$

$$\mathrm{TWIST} = q_{k,l} - q_{k-1,l} - q_{k,l-1} + q_{k-1,l-1}. \tag{17}$$

The stencil is rotated or reflected in an obvious way for flows at other angles ($c_x < 0$, $c_y < 0$, or both) and for the horizontal faces. Note that, for this particular basic scheme, $\hat{q}$ depends on the tangential Courant number (c_y in (11) through (17)), as well as the normal Courant number (c_x in (11) through (17)). Von Neumann stability analysis for this scheme [9] shows that it is stable for $|c_x| + |c_y| < 1$.

This upwind biased foward in time basic scheme was chosen in preference to, say, a high order centred in space and centred (leapfrog) in time scheme for two reasons. First, centred difference schemes have poor phase propagation characteristics leading to the production of (sometimes many) spurious extrema. Although the flux-limiter can suppress the production of spurious extrema, spurious changes of gradient (''staircasing'') can still arise. Second, when the basic scheme is centred in time the flux limiting procedure must, nevertheless, be forward in time, using values at time step $m - 1$ to constrain the fluxes used to calculate the values at $m + 1$. This necessitates a more complicated hybrid forward/centred time stepping. On top of this, the inclusion of source terms on the right of (1) or (2) then becomes problematical, because the values at time step m have ''seen'' more of the source than the values at time step $m - 1$.

For each of the schemes described in this paper a set of four very simple test cases is used to compare their basic properties. A doubly periodic square domain is covered by a regular grid of 31×31 boxes with $\Delta x = \Delta y$. Two different initial conditions are used: a Gaussian of standard deviation $3\Delta x$ and a square step profile of width $15\,\Delta x$ (Fig. 2). The grid and the Gaussian profile are identical to those used in [9], so that some of the results presented here can be compard directly with theirs. In the first two test cases these profiles are advected once around the domain (62 steps), left to right, by a constant velocity with Courant numbers $c_x = 0.5$, $c_y = 0$ in the x- and y-directions, respectively. In the third and fourth test cases the same two profiles are advected once around the domain (124 steps), diagonally, botton left to top right, by a constant wind with Courant numbers $c_x = 0.25$, $c_y = 0.25$.

Figure 3 shows the results of the four test cases for the basic advection scheme with no flux limiter. The scheme performs quite well on both the smooth Gaussian and the sharp square profile, although there is some smoothing of the sharp edges of the square profile. However, there are undershoots in all cases and overshoots in the square profile cases.

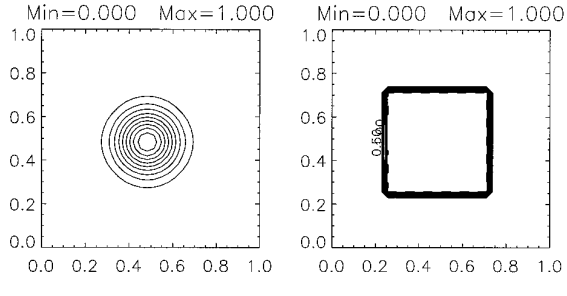

FIG. 2. Initial conditions for simple advection tests. The contour interval is 0.1: Left, circular Gaussian profile; right, square step profile.

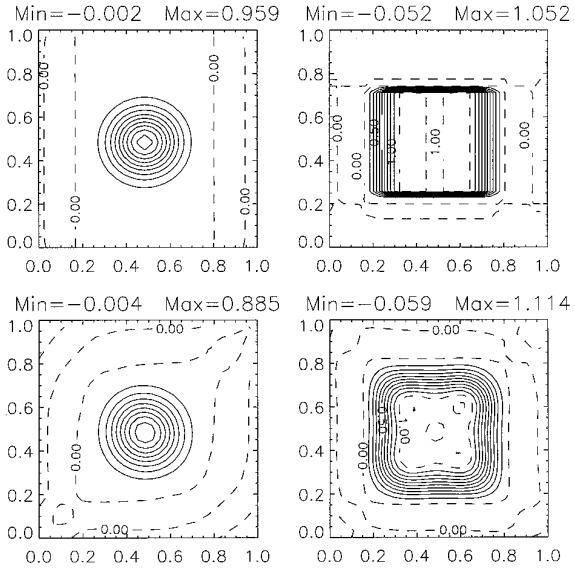

FIG. 3. Results of the four simple advection tests using the UTOPIA scheme without a flux limiter. The contour interval is 0.1. Contours less than or equal to 0 and contours greater than or equal to 1 are dashed. Upper left: Gaussian initial profile, flow left to right. Upper right: square initial profile, flow left to right. Lower left: Gaussian initial profile, diagonal flow. Lower right: square initial profile, diagonal flow.

3. ONE-DIMENSIONAL FLUX LIMITER

First the one-dimensional ''universal limiter'' [8] is reviewed here, using a notation that makes clear its later extension to higher dimensions. Then it is shown that applying a one-dimensional limiter separately in each coordinate direction gives unsatisfactory results, both allowing undershoots and overshoots and leading to distortion of the advected profile.

Consider part of a one-dimensional domain shown in Fig. 4, with the flow from left to right. Suppose a basic scheme has already been used to calculate interfacial mixing ratios, $\hat{q}_{\mathrm{L}}^{(\mathrm{basic})}$ and $\hat{q}_{\mathrm{R}}^{(\mathrm{basic})}$, at the faces marked L and R. The essence of the flux-limiting procedure is to ensure that the updated mixing ratio in gridbox k, q_k^{m+1}, lies within a certain range, $[(q_k^{m+1})_{\min}, (q_k^{m+1})_{\max}]$, by placing bounds on the total outflow from that box. (If a grid box has several outflow faces then there are many ways to satisfy the total outflow bounds by imposing individual outflow bounds at the different outflow faces. In this paper a simple procedure is chosen, that of allowing the same range of mixing ratio, $[\hat{q}_{\min}^{(\mathrm{out})}, \hat{q}_{\max}^{(\mathrm{out})}]$, at each outflow face of the box. More sophisticated choices are possible but have not been investigated.)

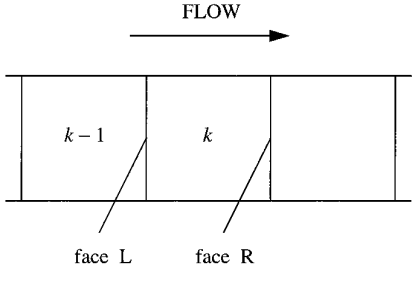

FIG. 4. Schematic showing grid boxes and faces involved in applying the one-dimensional universal limiter.

In order to calculate what the total outflow bounds must be, the possible range of total inflow must be known in advance. Therefore, the first step is to impose reasonably wide initial ''inflow'' bounds, $[(\hat{q}_{\mathrm{i}}^{(\mathrm{in})})_{\min}, (\hat{q}_{i}^{(\mathrm{in})})_{\max}]$ at each face, i. E.g., for the face marked L in Fig. 4,

(i) define the inflow bounds by

$$(\hat{q}_{\mathrm{L}}^{(\mathrm{in})})_{\min} = \min(q_{k-1}^{m}, q_k^{m}), \tag{18}$$

$$(\hat{q}_{\mathrm{L}}^{(\mathrm{in})})_{\max} = \max(q_{k-1}^{m}, q_k^{m}); \tag{19}$$

(ii) adjust the interfacial values given by the basic scheme to lie within these bounds:

$$\hat{q}_{\mathrm{L}}' = \min(\hat{q}_{\mathrm{L}}^{(\mathrm{basic})}, (\hat{q}_{\mathrm{L}}^{(\mathrm{in})})_{\max}), \tag{20}$$

$$\hat{q}_{\mathrm{L}}'' = \max(\hat{q}_{\mathrm{L}}', (\hat{q}_{\mathrm{L}}^{(\mathrm{in})})_{\min}). \tag{21}$$

In order to guarantee that q_k^{m+1} will lie within the range $[(q_k^{m+1})_{\min}, (q_k^{m+1})_{\max}]$ it will turn out to be necessary that

$$(q_k^{m+1})_{\min} \le (\hat{q}_{\mathrm{L}}^{(\mathrm{in})})_{\min}, \tag{22}$$

$$(q_k^{m+1})_{\max} \ge (\hat{q}_{\mathrm{L}}^{(\mathrm{in})})_{\max}. \tag{23}$$

A suitable choice is to

(iii) define $(q_k^{m+1})_{\min}$ and $(q_k^{m+1})_{\max}$ by

$$(q_k^{m+1})_{\min} = (\hat{q}_{\mathrm{L}}^{(\mathrm{in})})_{\min}, \tag{24}$$

$$(q_k^{m+1})_{\max} = (\hat{q}_{\mathrm{L}}^{(\mathrm{in})})_{\max}. \tag{25}$$

Note that this gives a suitable discrete analogue of the shape preservation property: $(q_k^{m+1})_{\min}$ and $(q_k^{m+1})_{\max}$ are the minimum and maximum mixing ratios in an upstream biased neighbourhood of box k.

Now suppose it could be guaranteed that the mixing ratio at the outflow face of box k, face R, will be greater than or equal to $(\hat{q}_{\mathrm{k}}^{(\mathrm{out})})_{\min}$. (Since $(\hat{q}^{(\mathrm{out})})_{\min}$ will later turn out to be the same for all outflow faces of box k, it has subscript k rather than R.) It would then follow that

$$q_k^{m+1} \le \frac{q_k^{m} + \tilde{c}_{\mathrm{L}}(\hat{q}_{\mathrm{L}}^{(\mathrm{in})})_{\max} - \tilde{c}_{\mathrm{R}}(\hat{q}_{\mathrm{k}}^{(\mathrm{out})})_{\min}}{1 + \tilde{c}_{\mathrm{L}} - \tilde{c}_{\mathrm{R}}}, \tag{26}$$

(provided that $1 + \tilde{c}_{\mathrm{L}} - \tilde{c}_{\mathrm{R}} > 0$; in fact a stronger condition

will be required later). So q_k^{m+1} will be less than or equal to $(q_k^{m+1})_{\max}$ if $(\hat{q}_k^{(\mathrm{out})})_{\min}$ is defined by

$$(q_k^{m+1})_{\max} = \frac{q_k^m + \tilde{c}_\mathrm{L}(\hat{q}_\mathrm{L}^{(\mathrm{in})})_{\max} - \tilde{c}_R(\hat{q}_k^{(\mathrm{out})})_{\min}}{1 + \tilde{c}_\mathrm{L} - \tilde{c}_\mathrm{R}}, \tag{27}$$

i.e.,

$$(\hat{q}_k^{(\mathrm{out})})_{\min} = \frac{q_k^m + \tilde{c}_\mathrm{L}(\hat{q}_\mathrm{L}^{(\mathrm{in})})_{\max} - (q_k^{m+1})_{\max}(1 + \tilde{c}_\mathrm{L} - \tilde{c}_\mathrm{R})}{\tilde{c}_\mathrm{R}}. \tag{28}$$

Similarly, q_k^{m+1} will be greater than or equal to $(q_k^{m+1})_{\min}$ provided that the mixing ratio at face R is less than or equal to $(\hat{q}_k^{(\mathrm{out})})_{\max}$, defined by

$$(\hat{q}_k^{(\mathrm{out})})_{\max} = \frac{q_k^m + \tilde{c}_\mathrm{L}(\hat{q}_\mathrm{L}^{(\mathrm{in})})_{\min} - (q_k^{m+1})_{\min}(1 + \tilde{c}_\mathrm{L} - \tilde{c}_\mathrm{R})}{\tilde{c}_\mathrm{R}}. \tag{29}$$

The final steps in the algorithm are, therefore,

(iv) calculate the outflow bounds for each face according to (28) and (29), and

(v) adjust the interfacial mixing ratio at each face to lie within the corresponding outflow bounds, e.g.,

$$\hat{q}_\mathrm{R}''' = \min(\hat{q}_\mathrm{R}'', (\hat{q}_k^{(\mathrm{out})})_{\max}). \tag{30}$$

$$\hat{q}_\mathrm{R} = \max(\hat{q}_\mathrm{R}''', (\hat{q}_k^{(\mathrm{out})})_{\min}). \tag{31}$$

The resulting values of $\hat{q}$ are substituted in (9) to step the mixing ratio.

In order for the algorithm to work, two conditions must hold. First, $(\hat{q}_k^{(\mathrm{out})})_{\min}$ must be less than or equal to $(\hat{q}_k^{(\mathrm{out})})_{\max}$. This will hold, provided that (22) and (23) hold and provided that the Courant number condition $\tilde{c}_\mathrm{R} < 1$ holds. Second, two sets of bounds are imposed at each face, the inflow bounds and the outflow bounds, and these bounds must not be mutually exclusive. In fact there always exists at least one value that satisfies both sets of bounds, namely the mixing ratio in the box upwind of the face in question, corresponding to a first-order upwind scheme.

Figure 5 shows the results of using the basic UTOPIA scheme combined with this one-dimensional limiter applied separately in each coordinate direction. For flow parallel to the grid this approach works well because each two-dimensional test effectively reduces to a set of one-dimensional tests, while the scheme reduces to the one-dimensional QUICKEST scheme [7] plus the one-dimensional universal limiter. However, for flow at an angle to the grid there is gross distortion of the advected profile and there are overshoots and undershoots.

The reason the scheme allows spurious extrema to arise can be illustrated as follows. Suppose a grid box contains a small mixing ratio, δ, and that neighbouring values are all greater than or equal to zero. The flux limiter will constrain the one-dimensional x-advection to decrease the mixing ratio by no more than δ, and the same is true for the y-advection. There is nothing to prevent the combined x-advection and y-advection from decreasing the mixing ratio by as much as 2δ and so producing negatives. To overcome the problem a fully multidimensional limiter is required; this is developed in the following section.

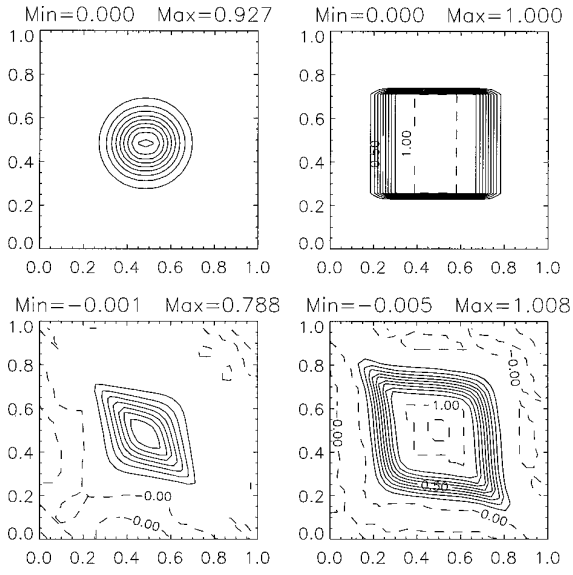

FIG. 5. As in Fig. 3, but for the UTOPIA scheme with the one-dimensional universal limiter applied separately in each coordinate direction.

4. MULTIDIMENSIONAL FLUX LIMITERS

4.1. *General Formulation*

The construction of the one-dimensional universal limiter in Section 3 suggests the following generalization to higher dimensions (Fig. 6). Note that this procedure does not depend on the grid used, or on the particular basic scheme used, so long as it is forward in time. Suppose that the basic scheme has been used to calculate a mixing ratio, $\hat{q}_i^{(\mathrm{basic})}$, for each face i.

As for the one-dimensional limiter, the first step is to impose reasonably wide initial inflow bounds, $[(\hat{q}_i^{(\mathrm{in})})_{\min}, (\hat{q}_i^{(\mathrm{in})})_{\max}]$ at each face, i. E.g., for the face marked I1 in Fig. 6.

(i) define the inflow bounds by

$$(\hat{q}_{\mathrm{I1}}^{(\mathrm{in})})_{\min} = \min(q_{\min}^{\mathrm{up}}, q_k^m), \tag{32}$$

$$(\hat{q}_{\mathrm{I1}}^{(\mathrm{in})})_{\max} = \max(q_{\max}^{\mathrm{up}}, q_k^m), \tag{33}$$

where $q_{\min}^{\mathrm{up}}$ is some minimum mixing ratio in an upstream neighbourhood of face I1, and $q_{\max}^{\mathrm{up}}$ is the corresponding maximum mixing ratio. The simplest possible choice is $q_{\min}^{\mathrm{up}} = q_{\max}^{\mathrm{up}} = q^{\mathrm{up}}$, although we shall find in Section 4.2 that improved results

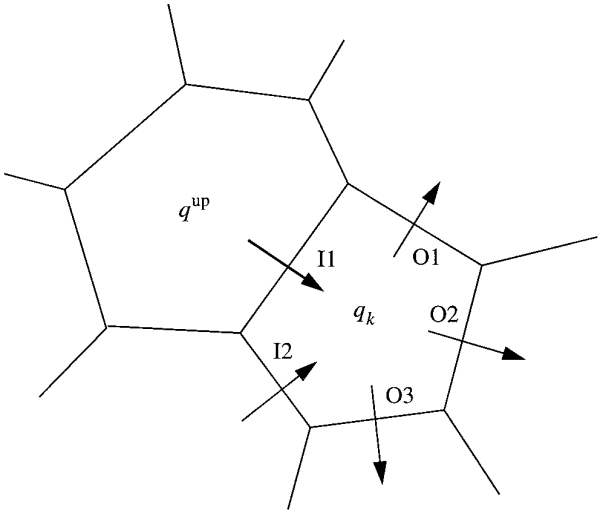

FIG. 6. Schematic showing some of the grid boxes and faces involved in applying the multidimensional limiter. The arrows indicate the direction of the normal component of the wind at the faces of box k. Faces I1 and I2 are inflow faces to box k. Faces O1, O2, and O3 are outflow faces of box k; q_k is the mixing ratio in box k; and q^{up} is the mixing ratio in one of the upwind boxes.

can be obtained by taking into account other boxes in the upstream neighbourhood.

(ii) Adjust the interfacial values given by the basic scheme to lie within these bounds:

$$\hat{q}'_{I1} = \min(\hat{q}^{(basic)}_{I1}, (\hat{q}^{(in)}_{I1})_{max}), \tag{34}$$

$$\hat{q}''_{I1} = \max(\hat{q}'_{I1}, (\hat{q}^{(in)}_{I1})_{min}). \tag{35}$$

The next step is to specify what range of values, $[(q_k^{m+1})_{min}, (q_k^{m+1})_{max}]$, will be allowed in box k at time step $m + 1$. In order to guarantee that q_k^{m+1} will lie within the range $[(q_k^{m+1})_{min}, (q_k^{m+1})_{max}]$ it will turn out to be necessary that

$$(q_k^{m+1})_{min} \le (\hat{q}_i^{(in)})_{min}, \tag{36}$$

$$(q_k^{m+1})_{max} \ge (\hat{q}_i^{(in)})_{max}. \tag{37}$$

for every inflow face, i, of box k. A suitable choice is to

(iii) define $(q_k^{m+1})_{min}$ and $(q_k^{m+1})_{max}$ by

$$(q_k^{m+1})_{min} = \min_i \{(\hat{q}_i^{(in)})_{min}\}, \tag{38}$$

$$(q_k^{m+1})_{max} = \max_i \{(\hat{q}_i^{(in)})_{max}\}, \tag{39}$$

where i runs over the inflow faces of box k. If box k has no inflow faces then $(q_k^{m+1})_{min}$ and $(q_k^{m+1})_{max}$ are set equal to q_k^m.

As for the one-dimensional limiter, $(q_k^{m+1})_{min}$ and $(q_k^{m+1})_{max}$ are the minimum and maximum mixing ratios in an upstream biased neighbourhood of box k, giving a suitable discrete analogue of the shape preservation property.

Now suppose it could be guaranteed that the mixing ratio at every outflow face of box k will be greater than or equal to $(\hat{q}_k^{(out)})_{min}$. It would then follow that

$$q_k^{m+1} \le \frac{q_k^m + \sum_{in} \tilde{c}_i (\hat{q}_i^{(in)})_{max} - \sum_{out} \tilde{c}_j (\hat{q}_k^{(out)})_{min}}{1 + \sum_{in} \tilde{c}_i - \sum_{out} \tilde{c}_j} \tag{40}$$

(provided that $1 + \sum_{in} \tilde{c}_i - \sum_{out} \tilde{c}_j > 0$). So q_k^{m+1} will be less than or equal to $(q_k^{m+1})_{max}$ if $(\hat{q}_k^{(out)})_{min}$ is defined by

$$(q_k^{m+1})_{max} = \frac{q_k^m + \sum_{in} \tilde{c}_i (\hat{q}_i^{(in)})_{max} - \sum_{out} \tilde{c}_j (\hat{q}_k^{(out)})_{min}}{1 + \sum_{in} \tilde{c}_i - \sum_{out} \tilde{c}_j}, \tag{41}$$

i.e.,

$$(\hat{q}_k^{(out)})_{min} = \frac{q_k^m + \sum_{in} \tilde{c}_i (\hat{q}_i^{(in)})_{max} - (q_k^{m+1})_{max}(1 + \sum_{in} \tilde{c}_i - \sum_{out} \tilde{c}_j)}{\sum_{out} \tilde{c}_j}. \tag{42}$$

Similarly, q_k^{m+1} will be greater than or equal to $(q_k^{m+1})_{min}$, provided that the mixing ratio at every outflow face of box k is less than or equal to $(\hat{q}_k^{(out)})_{max}$, defined by

$$(\hat{q}_k^{(out)})_{max} = \frac{q_k^m + \sum_{in} \tilde{c}_i (\hat{q}_i^{(in)})_{min} - (q_k^{m+1})_{min}(1 + \sum_{in} \tilde{c}_i - \sum_{out} \tilde{c}_j)}{\sum_{out} \tilde{c}_j}. \tag{43}$$

The final steps in the algorithm are, therefore,

(iv) calculate the outflow bounds for each face according to (42) and (43), and

(v) adjust the interfacial mixing ratio at each face to lie within the corresponding outflow bounds, e.g., for the face marked O1 in Fig. 6,

$$\hat{q}'''_{O1} = \min(\hat{q}''_{O1}, (\hat{q}_k^{(out)})_{max}), \tag{44}$$

$$\hat{q}_{O1} = \max(\hat{q}'''_{O1}, (\hat{q}_k^{(out)})_{min}). \tag{45}$$

Finally the values of $\hat{q}$ are inserted in Eq. (9) in order to update the grid box mixing ratios.

The inequalities (36) and (37), together with the Courant number condition $\sum_{out} \tilde{c}_j < 1$, ensure that $(\hat{q}_k^{(out)})_{min}$ is less than or equal to $(\hat{q}_k^{(out)})_{max}$. Also, there always exists at least one value that satisfies both the inflow bounds and the outflow bounds at any given face, namely the mixing ratio in the box upwind of that face, corresponding to a first-order upwind scheme.

The Courant number condition $\sum_{out} \tilde{c}_j < 1$ implies that not

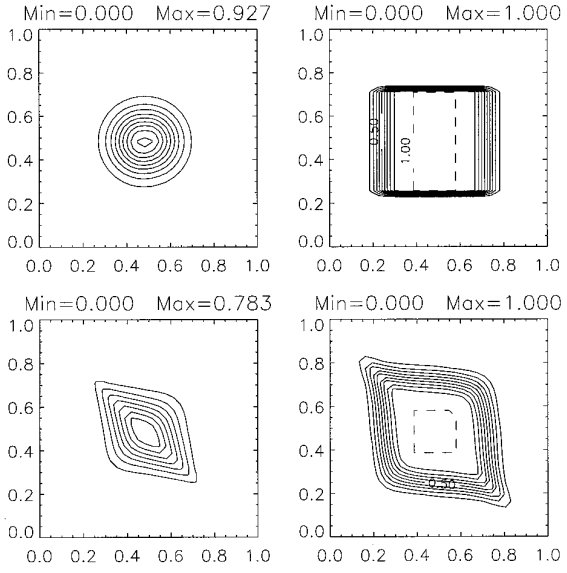

FIG. 7. As in Fig. 3 but for the UTOPIA scheme plus the simple form of the multidimensional limiter described in Section 4.1.

all of the fluid in a grid box may leave that grid box in one step. It ensures that the resulting scheme is shape-preserving and, therefore, stable in the sense that the global extremes of the mixing ratio cannot be amplied. In the tests carried out, the scheme tends to blow up quickly if $\sum_{\text{out}} \tilde{c}_j$ does become greater than 1.

Figure 7 shows the results of combining this limiter (with the simple choice $q^{\text{up}}_{\text{min}} = q^{\text{up}}_{\text{max}} = q^{\text{up}}$) with the UTOPIA basic scheme and applying the resulting scheme to the test cases of Section 2. The results confirm that the scheme is shape-preserving, i.e., there are no overshoots or undershoots. But for flow at an angle to the grid the advected profiles are badly distorted, with large spreading in the direction perpendicular to the flow.

4.2. *Refining the Limiter*

To understand the reason for the sideways spreading seen using the limiter of Section 4.1 it is useful to consider the idealized situation depicted in Fig. 8. The mixing ratio is 1 in the shaded region in the upper left and 0 elsewhere, and the wind is from the bottom left corner. The advected quantity spreads rapidly towards the bottom right because the mixing ratio in box C increases too rapidly. This, in turn, is because there is insufficient outflow from box C to box A.

The limiter of Section 4.1 causes this in two ways. First, the inflow bounds for box A require that $0 \le a \le 0$, i.e., $a = 0$. Obviously this constraint should be relaxed to allow for the fact that some fluid with higher mixing ratio can enter box C from the left, i.e., box A must be given some information about box B, which it meets only at the corner. Second, the minimum allowed value of q^{m+1}_{C} is 0, so that the outflow bound on a must be $a \le 0$ to allow for the worst case inflow, which could be $b = 0$ and $f = 0$. In practice, though, it is likely that the basic scheme value for b will be greater than 0, and this information can be used to calculate a less pessimistic worst case inflow mixing ratio and, hence, to relax the allowed range of outflow mixing ratios.

This suggests two refinements to the limiter. In the first refinement the inflow bounds for each face are widened by taking into account upstream-diagonal neighbours. For example, the refined inflow bounds on the value a in Fig. 8 are given by (32) and (33) with

$$q^{\text{up}}_{\text{min}} = \min(q_{\text{C}}, q_{\text{B}}) \tag{46}$$

$$q^{\text{up}}_{\text{max}} = \max(q_{\text{C}}, q_{\text{B}}). \tag{47}$$

(If there is inflow to box C from box D as well then q_{D} should also be included in the parentheses in (46) and (47). However, it is not necessary to include q_{F}.) For other grids, boxes in the upstream neighbourhood of the face in question, in addition to the box immediately upstream, can be taken into account on a similar way. E.g., see [14] for the case of a hexagonal grid.

The second refinement is more subtle. The inflow bounds ensure that the mixing ratio at an inflow face, i, of a box k lies in the range $[\min(q^{\text{up}}_{\text{min}}, q_k), \max(q^{\text{up}}_{\text{max}}, q_k)]$. The extremes of this range define the worst cases that the outflow bounds for box k must cope with. However, this estimate of the worst cases may be too pessimistic. In particular, once the basic scheme interfacial value has been adjusted to lie within this range, giving $\hat{q}''_i$, it can be shown that the outflow bounds for face i (face i is an outflow face for a neighbour of box k) will not move the final interfacial value outside the range $[\min(q^{\text{up}}_{\text{min}}, \hat{q}''_i), \max(q^{\text{up}}_{\text{max}}, \hat{q}''_i)]$. By using this narrower worst case range

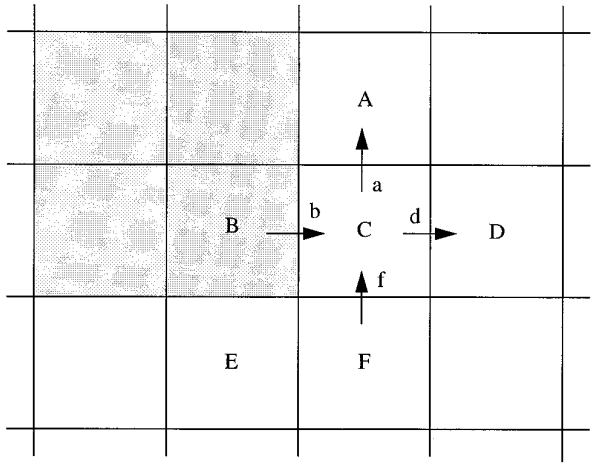

FIG. 8. Schematic illustrating the conditions under which the simple form of the multidimensional limiter can lead to distortion of the advected profile. The arrows indicate the direction of the normal component of the wind at the faces of box C; *a*, *b*, *d*, and *f* are mixing ratios at the faces of box C.

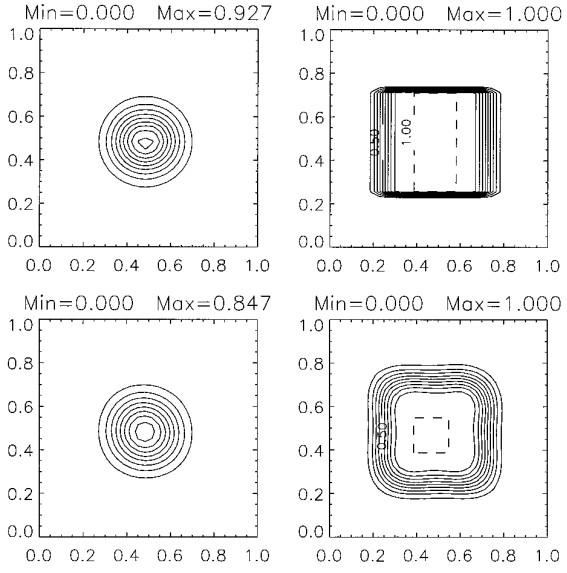

FIG. 9. As in Fig. 3 but for the UTOPIA scheme plus the multidimensional limiter including the refinements of Section 4.2.

for the inflow to box k, wider, less restrictive, outflow bounds are obtained. Thus, one extra step is required in the algorithm: after step (iii) the inflow bounds are revised:

$$(\hat{q}_i'^{(\mathrm{in})})_{\min} = \min(q_{\min}^{\mathrm{up}}, \hat{q}_i''), \tag{48}$$

$$(\hat{q}_i'^{(\mathrm{in})})_{\max} = \max(q_{\max}^{\mathrm{up}}, \hat{q}_i''), \tag{49}$$

for every face i, and the revised bounds are used in (42) and (43) in place of $(\hat{q}_i^{(\mathrm{in})})_{\min}$ and $(\hat{q}_i^{(\mathrm{in})})_{\max}$ to calculate the outflow bounds in step (iv).

Neither of these refinements on its own relieves the grid-flow angle-dependent distortion shown in Fig. 7, but when they are used together the resulting scheme performs well and any remaining distortion is negligible (Fig. 9).

5. SPLIT CYLINDER TEST

All of the results presented so far use a flow that is constant in space and time to highlight the most basic behaviour of the advection schemes. One further result is presented here that tests the refined flux-limited scheme for a flow constant in time but not in space. Further tests of a similar scheme under straining flow and a discussion of the dissipation associated with the scheme when there are cascades to small scales are presented elsewhere [14].

The test is the advection of a split cylinder by a solid body rotation as used by Zalesak [16]. The domain is 100×100 grid boxes ($\Delta x = \Delta y$) with a counterclockwise solid body rotation centred on box (50, 50). A cylinder of radius 15 Δx, from which a slot of width 5 Δx has been cut, is initially centred at grid box (50, 75). The maximum extent of the ''bridge'' joining the two halves of the cylinder is 5 Δx. The rotation rate and time step are chosen so that the cylinder should return to its initial position after 628 steps.

The initial and final profiles are shown in Fig. 10. The maximum and minimum values are accurately preserved, although there is some erosion of the ''bridge'' and filling of the slot. This solution is slightly more diffused than that presented in [16]. This is because of the slightly diffusive nature of the upwind biased basic scheme used here. When the FCT algorithm is used with the same basic scheme the results are virtually identical to those in Fig. 10 (not shown).

6. FLUX LIMITER FOR FLUID DENSITY

So far this paper has addressed the problem of how to timestep the mass mixing ratio of an advected scalar, given the mass fluxes of the fluid. The two forms of the advection equation, (1) and (2), imply different properties of advection, namely conservation and shape preservation, that can be obtained in a numerical advection scheme by discretizing the flux form and by using an appropriate flux limiter.

This section addresses the problem of how to timestep the fluid density (or an anlogous quantity such as fluid depth in the shallow water equations), given the fluid velocity. There is only one form of the mass continuity equation (4), so at first it may seem that we can demand conservation of mass from a numerical scheme, but no analogue of the shape preservation property. However, it is possible to imagine a nondivergent flow in which a scheme without a flux limiter would allow spurious extrema to arise in the density, so in this case we can demand an analogue of the shape preservation property and there is a role for a flux limiter. More generally, the idea of shape preservation must be extended to apply to density in divergent flows.

Equation (4) can be rewritten as

$$\frac{D\rho}{Dt} + \rho \nabla \cdot \mathbf{v} = 0, \tag{50}$$

which implies that extrema in the density can increase or decrease and new extrema can arise, depending on the divergence. Discretizing in time *following a fluid parcel* gives

$$\rho^{n+1} \approx \rho^n (1 - \Delta t \nabla \cdot \mathbf{v}). \tag{51}$$

This suggests a way to place bounds on the allowed values of density after one time step. If q is replaced by ρ and $\tilde{c}$ is replaced by c in (32) through (45) and the resulting values of $\hat{\rho}$ are substituted in (5) to step the density, the new density in grid box k is guaranteed to lie in the range

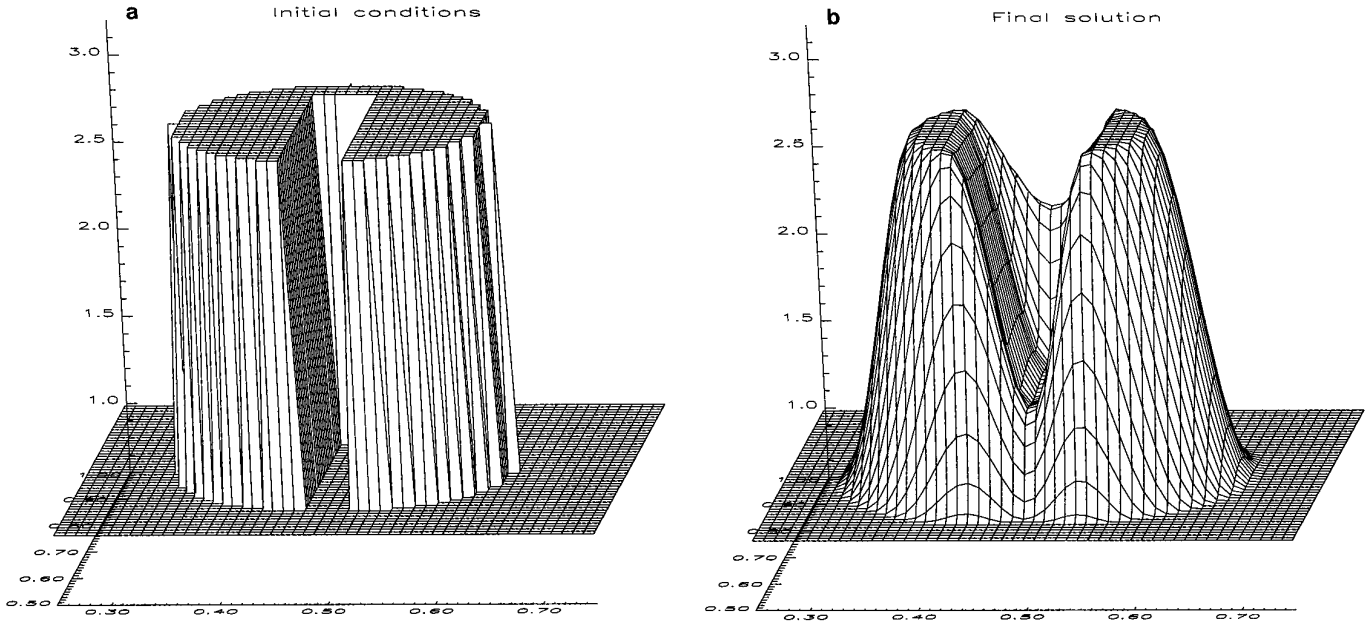

FIG. 10. Perspective view of the initial conditions and final solution of the split cyclinder test. Initially the mixing ratio is 3.0 in the split cylinder and 1.0 elsewhere. Only a subregion (50 boxes by 50 boxes) around the cyclinder is shown.

$$\left[(\rho_k^{m+1})_{\min} \left(1 + \sum\nolimits_{\text{in}} c_i - \sum\nolimits_{\text{out}} c_j \right), (\rho_k^{m+1})_{\max} \left(1 + \sum\nolimits_{\text{in}} c_i - \sum\nolimits_{\text{out}} c_j \right) \right]. \tag{52}$$

That is, the new density is bounded by the density at the previous time step in some upstream neighborhood after making appropriate allowance for the divergence. ($(\rho_k^{m+1})_{\min}$ should not be interpreted as the minimum permitted value of ρ in box k at step $m+1$. It is simply the smallest value of ρ in some upstream biased neighbourhood of box k at step m. Similar comments apply to $(\rho_k^{m+1})_{\max}$.) Thus the flux limiter algorithm of Section 4.1 can be applied to fluid density with only a very minor modification. The refinements of Section 4.2 also carry over in a trivial way.

This flux limiter has been applied successfully to the equation for fluid depth in the shallow water equations [14].

It is not clear how to extend this flux limiter to other quantities, like momentum, unless an analogue of the shape preservation property can be found. The flux limiter can be applied to potential vorticity in a stratified rotating fluid because it satisfies the same advection equations as the mixing ratio of an inert scalar. Again, see [14] for an application to the shallow water equations.

7. SUMMARY AND DISCUSSION

7.1. *Summary of Results*

A general framework has been developed for building multidimensional shape-preserving advection schemes using flux limiters on arbitrary grids for either compressible or incompressible flow. A scheme with the simplest form of the flux limiter can distort the advected profile, depending on the flow orientation relative to the grid, but a scheme with a refined version of the limiter gives satisfactory results. The refinements involve (i) using diagonal-upstream neighbouring boxes, as well as immediately adjacent upstream boxes, to specify the inflow bounds and (ii) using information about the basic scheme box-face mixing ratios to relax the outflow bounds. The method can be applied to the advection of a scalar such as the mass mixing ratio of a chemical constituent and also to the mass continuity equation for the density of the fluid itself.

7.2. *Other Grids*

All of the results presented in this paper use a regular square grid. The flux limiter described here has also been applied successfully on a regular hexagonal grid [14] and on a hexagonal–icosahedral grid (i.e., a grid made up of hexagons and pentagons) on a sphere. The limiter of Section 4.1 and the second refinement of Section 4.2 apply without modification to arbitrary grids. A variation of the first refinement of Section 4.2 may be made by using appropriate upstream-sideways neighbours to give wider inflow bounds; the details obviously depend on the grid used. The first refinement appears to be necessary on all of the grids tried to avoid distortion of the advected profiles. Interestingly, the second refinement appears to be unnecessary on a hexagonal grid, although there is no harm in retaining it.

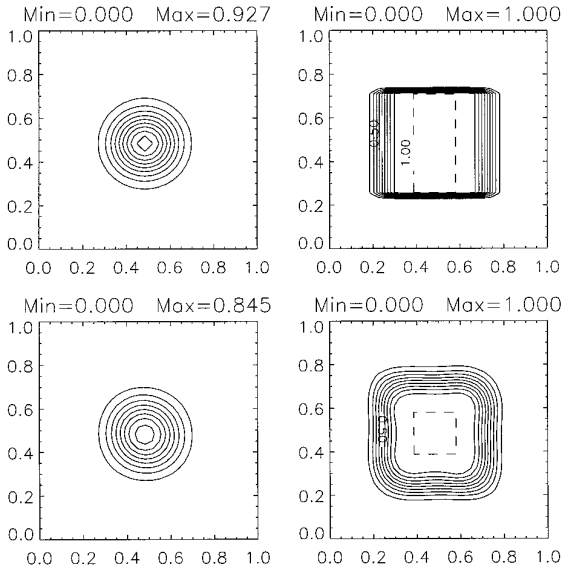

FIG. 11. As in Fig. 3 but for the UTOPIA scheme modified using the multidimensional FCT algorithm.

7.3. *Comparison with FCT*

The new algorithm for multidimensional flux limiters presented here is similar in several ways to the multidimensional FCT algorithm. Both methods involve looking in the neighbourhood of a grid box to define the minimum and maximum permitted values in that box one step later. Both methods attempt to modify the fluxes as little as possible while still being able to guarantee shape preservation. Both methods rely on the fact that there always exists at least one solution for the limited fluxes, namely those given by a low order upwind scheme (for FCT this means that the antidiffusive flux is zero). And both methods distinguish between inflow faces of a grid box and outflow faces (for FCT the distinction is between faces having inward and outward antidiffusive fluxes). There are also differences between the two methods. The algorithm presented here does not involve the calculation of an intermediate transported/diffused field; instead, it involves the calculation of intermediate values of the fluxes, which are subsequently modified. Also, the algorithm presented here deals directly with the full fluxes, rather than separately treating the antidiffusive component of the fluxes.

The numerical results of applying FCT to the basic scheme of Section 2 are very similar to those using the new flux limiter. See Fig. 11 and compare Fig. 9. The low order scheme used for this test was first-order upwind (donor cell).

The cost of the new flux limiter appears to be similar to the cost of FCT. For example, the split cylinder test required 944 s of CPU for the basic scheme with no flux limiter, 1481 s for the new flux-limited scheme, and 1394 s for the basic scheme with FCT. It is also worth noting that the code for the new flux limiter can be written so as to ''vectorize'' on computers with a pipeline architecture.

The algorithm presented here puts single stage flux-limited schemes on a par with two-stage FCT schemes in terms of flexibility, allowing the construction of genuinely multidimensional schemes for compressible and incompressible flow on arbitrary grids. The performance of the flux-limited and FCT schemes compares well in the tests presented here. Flux-limiting now appears to be a viable alternative to FCT for building multidimensional, conservative, shape-preserving advection schemes.

ACKNOWLEDGMENTS

This work was carried out under the UK Universities Global Atmospheric Modelling Programme (UGAMP) which is funded by the UK Natural Environment Research Council, partly through contract PECD 7/12/83 with the UK Department of the Environment. The comments of several anonymous reviewers led to improvements in this manuscript.

REFERENCES

1. R. Bleck, and D. B. Boudra, *J. Geophys. Res.* **91,** 7611 (1986).
2. D. L. Book, J. P. Boris, and K. Hain, *J. Comput. Phys.* **18,** 248 (1975).
3. J. P. Boris, and D. L. Book, *J. Comput. Phys.* **11,** 38 (1973).
4. J. P. Boris, and D. L. Book, *J. Comput. Phys.* **20,** 397 (1976).
5. A. Bott, *Mon. Weather Rev*. **121,** 2638 (1993).
6. R. C. Easter, *Mon. Weather Rev*. **121,** 297 (1993).
7. B. P. Leonard, *Comput. Method Appl. Mech. Eng.* **19,** 59 (1979).
8. B. P. Leonard, *Comput. Methods Appl. Mech. Eng.* **88,** 17 (1991).
9. B. P. Leonard, M. K. MacVean, and A. P. Lock, NASA Technical Memorandum 106055 ICOMP-93-05, 1993 (unpublished).
10. A. G. Petschek, and L. D. Libersky, *Mon. Weather Rev*. **103,** 1104 (1975).
11. P. J. Rasch, *Mon. Weather Rev*. **122,** 1337 (1994).
12. P. K. Smolarkiewicz, and W. W. Grabowski, *J. Comput. Phys.* **86,** 355 (1990).
13. P. K. Sweby, in *Lectures in Appl. Math.*, Vol. 22 (Am. Math. Soc., Providence, RI, 1985), p. 289.
14. J. Thuburn, *Mon. Weather Rev.*, **123,** 1888 (1995).
15. B. Van Leer, *J. Comput. Phys.* **14,** 361 (1974).
16. S. T. Zalesak, *J. Comput. Phys.* **31,** 335 (1979).